Article

Chemical Bond Modification Upon Phase Transformation of TiO Nanoribbons Revealed by Nanoscale X-ray Linear Dichroism

Peter Krueger, Melita Sluban, Polona Umek, Peter Guttmann, and Carla Bittencourt

J. Phys. Chem. C, **Just Accepted Manuscript** • DOI: 10.1021/acs.jpcc.7b06968 • Publication Date (Web): 19 Jul 2017

Chemical Bond Modification upon Phase Transformation of TiO_2 Nanoribbons Revealed by Nanoscale X-ray Linear Dichroism

Peter Krüger,*,†,‡ Melita Sluban,¶,§ Polona Umek,¶ Peter Guttmann,‖ and Carla Bittencourt⊥

† *Graduate School of Science and Engineering, Chiba University, Chiba 263-8522, Japan*

‡ *Molecular Chirality Research Center, Chiba University, Chiba 263-8522, Japan*

¶*Jožef Stefan Institute, Jamova cesta 39, SI-1000 Ljubljana, Slovenia*

§ *Jožef Stefan International Postgraduate School, Jamova cesta 39, SI-1000 Ljubljana, Slovenia*

‖*Helmholtz-Zentrum Berlin für Materialien und Energie GmbH, Research group X-ray microscopy, Albert-Einstein-Str. 15, D-12489 Berlin, Germany*

⊥*Chimie des Interactions Plasma Surface, CIRMAP, University of Mons, 23 Place du Parc, B-7000 Mons, Belgium*

E-mail: pkruger@chiba-u.jp

Abstract

Titanium dioxide in the TiO_2-B phase, which can be stabilized in nanoparticle form, is a promising anode material for lithium ion batteries. Here the structural and electronic changes between nanoribbons in TiO_2-B and the thermodynamic stable anatase phase are studied using nanoscale X-ray absorption spectroscopy and first principles calculations. The oxygen K-edge spectra of the two phases display marked

differences which are very well reproduced in the calculations. Strong linear dichroism is observed in single nanoribbons, reflecting preferential O-2p to Ti-3d bond orientation in the low symmetry crystal structures. A simple bond counting model is developed which semi-quantitatively accounts for the major dichroic effect. It is shown that the crystal orientation of the nanoparticles can be inferred from the dichroic spectra.

Introduction

Elongated TiO_2 particles with large aspect ratios, such nanotubes,[1] nanowires[2] and nanoribbons[3,4] have anisotropic transport properties and a high surface to bulk ratio, which makes them promising materials for optoelectronics and catalytic applications. Like their bulk counterparts, TiO_2 nanostructures exist in different crystallographic phases including anatase, rutile and TiO_2-B (bronze). The TiO_2-B phase has attracted considerable attention as an anode material for lithium ion batteries[5] especially in the form of nanowires.[2] The rather open TiO_2-B crystal structure contains channels[6] which contribute to high capacitance and ion mobility.[7] Bulk-like TiO_2-B single crystals are unstable and thin films could be synthesized only very recently.[8] Especially in view of device applications, where different phases may coexist and TiO_2-B particles may transform to the thermodynamic stable anatase phase, it is important to identify and understand the structural and electronic differences between these two phases.

Here we have studied the electronic structure of TiO_2 nanoribbons in TiO_2-B and anatase phases using polarization dependent near-edge X-ray absorption fine structure spectroscopy (NEXAFS)[9] in the transmission X-ray microscope (TXM)[10] and density functional theory (DFT). The NEXAFS spectra of single nanoparticles display strong linear dichroism and the dominant effect is the variation of the intensity ratio between the two lowest energy peaks pertaining to Ti-3d derived states. We show that this is a direct consequence of the directional Ti-O bonding and propose a simple model that explains and reproduces the observed intensity ratio variation. Moreover, the crystal orientation in the nanoribbons is

found by comparing the experimental and calculated dichroic spectra.

Experimental and Computational Methods

Sample preparation and characterization. Titania nanoribbons have been prepared by calcining $H_2Ti_3O_7$ nanoribbons (HTiNRs),[11,12] whose synthesis is described elsewhere.[3,13] Here, titania nanoparticles in the TiO_2-B and anatase phase were obtained by heating the HTiNR precursor in static air at 400 °C and 650 °C, respectively. The shape of the particles does not change during this process. The morphology of the samples was studied using transmission electron microscopy (TEM) and the crystal structure was determined using powder X-ray diffraction. NEXAFS spectra were recorded at room temperature in transmission mode with the TXM at the U41-XM beamline of the BESSY II synchrotron, Berlin,[10] with a calculated spectral resolution of $E/^{\circ}E = 20000$. The spectra were normalized by using the signal intensity in the proximity of the sample to correct for intensity variations with photon energy and acquisition time. The polarization dependence was controlled by rotating the sample. See the Supporting Information for further details.

Density functional calculations. The electronic structures of TiO_2-B and anatase were calculated using density functional theory in the local density approximation with the Vienna ab initio simulation package.[14] Projector-augmented wave potentials were employed with O-2s and Ti-3p treated as valence shells. The energy cutoff was set to 500 eV and the Brillouin zones of TiO_2-B and anatase were sampled on a $4\times12\times8$ and a $12\times12\times8$ mesh, respectively. The experimental structures of the bulk crystals were used.[6] As in our previous studies on TiO_2 anatase[15] and (Na,H) titanates[16,17] the O K-edge spectra were obtained from the density of unoccupied states projected on p-type orbitals centered on the oxygen sites. Core-hole effects were neglected since they are known to be weak for the O-K edge of TiO_2.[18] Finite lifetime of the X-ray absorption final state was accounted for through Lorentzian broadening with an energy-dependent width $\Gamma(E) = \Gamma_c + A(0.5 + \arctan[(E - E_0)/b]/\pi)$.

The same parameter values as for anatase[15] were used, namely $\Gamma_c = 0.156$ eV (core-hole width), $A = 1$ eV, $b = 2$ eV and $E_0 = 12.7$ eV (plasmon peak). The calculated spectra were rigidly shifted in energy (individually for each TiO_2 phase) such as to align the absorption threshold with experiment.

Results and Discussion

X-ray absorption spectra of TiO_2-B and anatase nanoribbons

The TiO_2 nanoribbons are 1–4 μm long with lateral dimension ranging from 30 to 250 nm.[13,19] The TEM image of a typical nanoribbon in the TiO_2-B phase (Fig. 1 c) reveals its characteristic porous surface.[13,20,21] Both in the anatase and TiO_2-B crystal structures (Fig. 1),

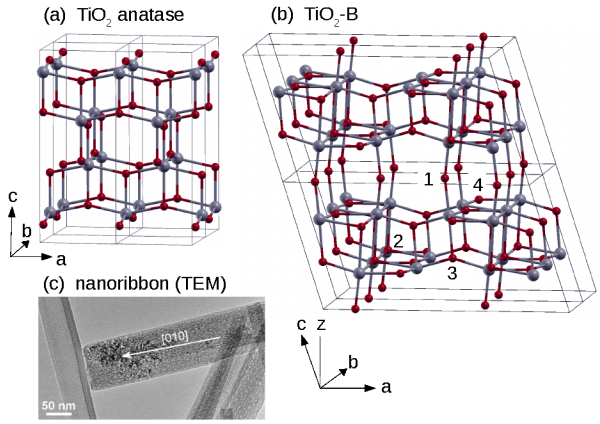

Figure 1: Ball and stick models of (a) anatase and (b) TiO_2-B crystal structures. Ti and O as big gray and small red balls, respectively. In TiO_2-B (b) the inequivalent O sites are labeled 1–4. (c) TEM image of a typical nanoribbon in TiO_2-B phase.

the Ti atoms sit at the centers of distorted TiO_6 octahedra. The local structure around the O sites is very different, however. In TiO_2-B there are four inequivalent O sites, with Ti-coordination between two and four, while in anatase all O sites are equivalent and three-fold coordinated. To understand the electronic structure changes induced by the TiO_2-B to anatase phase transformation we have measured the NEXAFS of bundles of randomly

oriented nanoribbons (Fig. 2). The Ti L_{23}-edge spectra of the two phases (Fig. 2 a,b) are

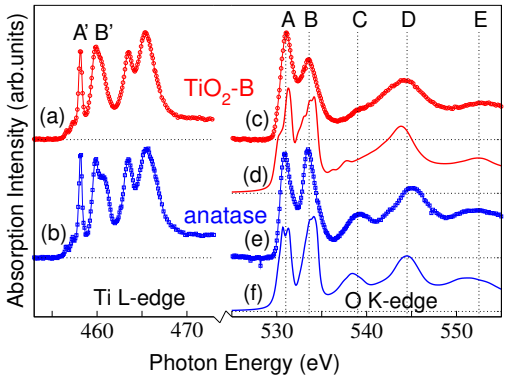

Figure 2: Experimental Ti L-edge (a,b) and O K-edge (c,e) absorption spectra of randomly oriented nanoribbons in TiO_2-B (a,c) and anatase (b,e) phase. (d,f) Calculated spectra.

very similar reflecting the common TiO_6 coordination. Small differences are observed in the relative peak intensities and the shape of the B′ peak. The sharp A′ peak corresponds to transitions from Ti-$2p_{3/2}$ to 3d-t2g states. The Ti-t2g orbitals point between the oxygen neighbors and form rather weak π^*-bonds with O-2p. Conversely, the broad B′ feature corresponds to transitions into Ti 3d-eg orbitals which point directly to the oxygen neighbors and which form stronger σ^*-bonds. Therefore, the shape of the B′ ("L3-eg") feature is more sensitive to the symmetry at the cation site and can be used as a fingerprint of the various titanium oxide compounds.[22] Previously we have shown that the splitting of the L3-eg peak is related to the connectivity of the TiO_6 octahedra.[16,23] It increases with the O-Ti coordination number N between zero splitting for N=2 ($SrTiO_3$) to about 1 eV for N=3 (rutile and anatase TiO_2).[23] TiO_2-B has four inequivalent O sites with coordination numbers N=2,3,3,4 (see Figs 1 b and 4) resulting in an average of N=3. Thus we expect TiO_2-B to have the same splitting as anatase, which is approximately observed experimentally (Fig. 2 a,b).

The electronic structure differences between the two phases are more clearly visible in the O K-edge spectra (Fig. 2 c,e). The spectra of both phases display a five-peak structure with two sharp peaks at 531.0 (A) and 533.6 eV (B) and three broad features at about 539 (C), 544.5 (D) and 552.5 eV (E). In TiO_2-B, the A:B peak intensity ratio is larger than in

anatase, peak D is shifted to lower energy by about 0.5 eV and peak C is strongly suppressed. It is well known for anatase,[24] that peaks A and B derive correspond to Ti-3d t2g and eg dominated states which form π*- and σ*-antibonding states with O-2p, respectively. The higher energy peaks C, D and E have been attributed to more delocalized states involving hybridization of O-p with Ti-sp and O-p orbitals on other sites.[15,24]

We have calculated the O K-edge spectra for the two TiO_2 crystal phases with density functional theory. The spectra for unpolarized light, corresponding to a powder sample, are shown in Fig. 2 d,f. The overall agreement with experiment is very good in both phases. The calculated A:B intensity ratio is slightly underestimated and energies of peaks C–E are too low by 0.5–1 eV. This might be due to the neglect of the core-hole effect, which often leads to some intensity increase of the lowest energy peak and small changes in peak positions. Perfect agreement of the intensities is not expected because the randomly oriented nanoribbons keep a preferential in-plane orientation on the support grid for the TXM experiments, as observed in other nanostructures.[9] Then, considering the strong linear dichroism of the individual ribbons (see below) the data is not fully equivalent to a powder sample. Importantly, however, all differences between the TiO_2-B and the anatase spectra (change of A:B ratio, shift of peak D and suppression of peak C) are reproduced in the calculations, demonstrating that the O K-edge NEXAFS is a reliable measure of the O-p projected density of unoccupied states in titania.[16]

Polarization dependent O K-edge spectra of individual nanoribbons

We now focus on the polarization dependent spectra of individual nanoribbons which provide insight into their anisotropic electronic structure.[17] The experimental geometry is schematically shown in Fig. 3 f. The NEXAFS spectra are recorded with two orthogonal linear polarizations, either parallel (Y) and perpendicular (X) to the long ribbon axis (L_Y). We have selected nanoribbons that appear bright, uniform and rather wide in the TXM image (Fig. S3 in the Supporting Information). A nanoribbon is brightest when the cross section

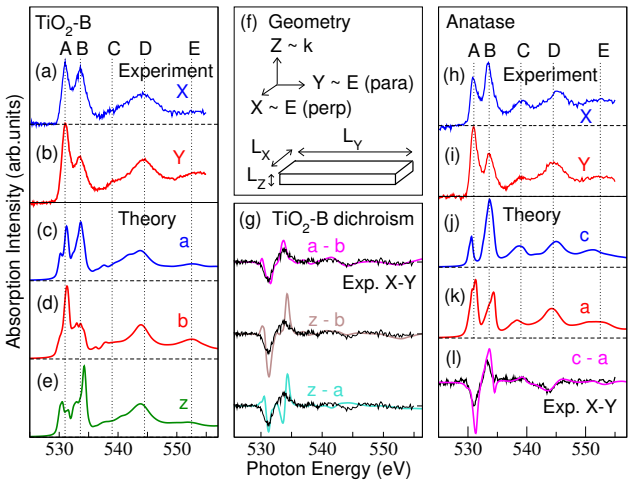

Figure 3: Linear polarization dependent O K-edge spectra of single nanoribbons in TiO_2-B (a-e,g) and anatase (h-l) phase. The experimental polarization (E) is chosen across (X) or along (Y) the long dimension of the nanoribbon, see (f). The theoretical polarization is taken along the crystal axes **a**, **b**, **c** or **z**. For curves Exp.X-Y in (g,l) a linear background subtraction and equal area normalization was done on X, Y before taking their difference.

is smallest, that is, when light incidence (k) is along the short dimension (L_Z). From this we infer that the selected ribbons lie essentially flat on the XY plane and that parallel (Y) and perpendicular (X) polarization directions correspond to the ribbon dimensions L_Y and L_X, respectively. The polarization dependence of the Ti L-edge spectra is very weak and not shown. At the O K-edge of TiO_2-B however, the experimental spectra for perpendicular (X) and parallel (Y) polarization differ strongly and the largest variation is in the A:B intensity ratio, see Fig. 3 a,b. Also in the calculations, the A:B intensity ratio is dramatically different for polarization along the three crystal axis (Fig. 3 c-e). It is obvious that the calculated **b**-axis spectrum corresponds to the experimental Y polarization. Further, the experimental X direction can be assigned to the **a**-axis, because the calculated **a**-spectrum agrees much better with the experimental X-spectrum than the **z**-spectrum, both in terms of A-B splitting and intensity ratio. The correspondence X=a, Y=b is even more evident in the dichroic spectra (Fig. 3 g). We have thus clearly identified the orientation of the crystal axes in single TiO_2-B nanoribbons from the polarization dependence of the NEXAFS spectra.

For further insight in the local electronic structure of the nanoribbons, we have calculated

the polarization dependent O K-edge spectra (Fig. 4) for each of the inequivalent O sites O1–4 in TiO_2-B. Site O1 has a linear Ti-coordination along the **z**-axis. O2 is a tetrahedral

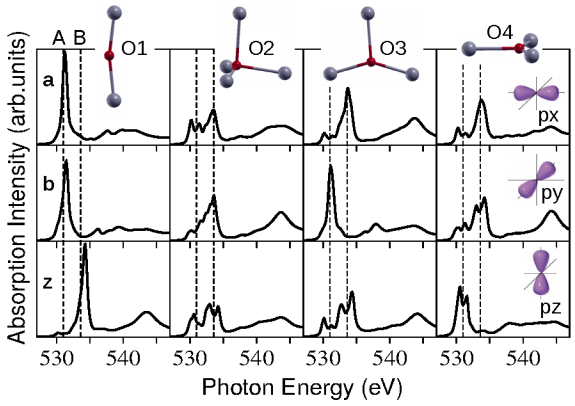

Figure 4: Calculated O K-edge spectra of TiO_2-B for the four O sites and light polarization along **a**, **b**, **z** axes. The Ti coordination of each O site is shown at the top. The experimental A, B peak energies of Fig. 2 are indicated by dotted lines.

site, while O3 and O4 have triangular Ti coordination in the xz and xy planes, respectively. We refer to the spectra as On-q, where n=1–4 is the number of the O site and q=a,b,z is the light polarization. The calculated A:B peak intensity ratio is strongly polarization and site dependent. This reflects the directional O-2p to Ti-3d bonding of the different O sites. For example, the O1-z spectrum displays a sharp, intense B peak but no A peak. This is because the O1-pz orbital forms σ bonds with the Ti-eg orbitals (peak B) of the Ti neighbors above and below but it cannot, by symmetry, hybridize with Ti-t2g (peak A). Reversely, O1-px,y can only hybridize with Ti-t2g and so the O1-a,b spectra have a strong A-peak and no B-peak. This also applies to O3-py and O4-pz orbitals which, being perpendicular to the O-Ti3 triangular plane, can make only π-bonds with the Ti neighbors. In all other cases, both σ and π bonds are possible by symmetry, so peaks A and B both have finite intensity.

Analysis of linear dichroism with bond counting model

Here we show that the site and polarization dependence of the A:B intensity ratio can be explained with a simple bond counting model. In titania, peak B is due to O-p orbitals that are hybridized via σ^*-bonds with Ti 3d-eg states, and so its intensity (I_B) is roughly proportional to the number of O-Ti σ-bonds (n_σ) as we have shown for titanate nanotubes.[16] Thus we have $I_B \approx \alpha n_\sigma$, where α is a constant. In the present case of polarization dependent spectra, where specific orbital symmetries (O-px,y,z) are selected, we need to take n_σ as the number of σ bonds per symmetry equivalent O-p orbital. The tetrahedral O2 site has four σ bonds. In perfect tetrahedral symmetry all three O-p orbitals are equivalent, so n_σ=4/3. For a triangular site (O3 or O4), n_σ=3/2 and n_σ=0 for in-plane and out-of-plane O-p orbitals, respectively. We now estimate the proportionality factor α. The intensity of peak A (I_A) increases with the number of O-Ti π-bonds. We observe from Fig. 4, that the sum I_A+I_B is about constant, i.e. independent of oxygen site and light polarization. For the O1-pz orbital, we have I_A=0 and n_σ=2, so $\alpha \equiv I_B/n_\sigma = (I_A + I_B)/2$. As $I_A + I_B$ is constant, we get, in general, $I_B = (I_A + I_B)n_\sigma/2$, or equivalently, I_A:$I_B = (2 - n_\sigma) : n_\sigma$. The prediction of this model is shown in Table 1. By comparison with Fig. 4 it can be seen that this simple model accounts surprisingly well for the A:B intensity ratios as obtained from DFT. Most importantly, the O-site averaged intensity ratio ("average") is predicted to be largest for b polarization, followed by a and z polarizations, in excellent agreement with the spectra in Fig. 3 c-e. The peak intensity ratios of the experimental spectra (Fig. 3 a,b) were estimated by fitting the A-B spectral region with two asymmetric Gaussians (asymmetry parameter set to 1.5) after linear background subtraction. The result is I_A:I_B=45:55 for perpendicular (X) polarization and I_A:I_B=60:40 for parallel (Y) orientation, which agrees well with the O-averaged I_A:I_B values in Table 1 for a and b polarization, respectively. This confirms our axis assignment (X∼a, Y∼b) again and shows that the linear dichroism of TiO_2-B in the low energy region at the O K-edge spectra can be explained with our simple bond counting model.

Table 1: Bond counting model results for TiO_2-B, sites O1–4 and polarizations a,b,z.

	n_σ = # of O-Ti σ-bonds					I_A:I_B=(2−n_σ):n_σ				
	O1	O2	O3	O4	average	O1	O2	O3	O4	average
a	0	4/3	3/2	3/2	26/24	1:0	1:2	1:3	1:3	46:54
b	0	4/3	0	3/2	17/24	1:0	1:2	1:0	1:3	65:35
z	2	4/3	3/2	0	29/24	0:1	1:2	1:3	1:0	40:60

For the anatase phase, the polarization dependent NEXAFS spectra of a single nanoribbon are shown in Fig. 3 h,i. From the comparison with the DFT calculated spectra (Fig. 3 j,k) it is evident that the experimental X polarization corresponds essentially to the crystal **c** axis and the Y polarization to the **a** axis (or, by tetragonal symmetry, to any other axis in the ab-plane). Not only the low energy A,B peaks but also the higher energy regions show substantial linear dichroism which is well reproduced in the calculations with the assignment X=c, Y=a. The calculated dichroism in the A-B energy region is some 20–50% larger than the measured one, which suggests that the Y polarization direction is not fully aligned with the anatase c-axis.

The observed linear dichroism in the A-B energy region can be understood with the bond counting model introduced above. In anatase, all O sites are equivalent and have a triangular Ti coordination, see Fig. 1 a. Consider a OTi3 triangle in the ac-plane. Since this is the same coordination as O3 in TiO_2-B, we have, from Table 1, n_σ=0, I_A:I_B=1:0 for b-polarization and n_σ=3/2, I_A:I_B=1:3 for a- or c-polarization. By taking the O site average with a=b in the tetrahedral symmetry, we find n_σ=3/4, I_A:I_B=5:3 for polarization in the ab-plane, and n_σ=3/2, I_A:I_B=1:3 for polarization along the **c**-axis. It can be seen from Fig. 3 j,k, that these polarization dependent A:B intensity ratios agree very well with the DFT calculated spectra. The experimental intensity ratios are I_A:I_B=40:60 for perpendicular (X) and 58:42 for parallel (Y) polarization, which agrees fairly well with the ratios 25:75 for c-polarization and 63:37 for (a,b)-polarization, respectively, obtained from the bond counting model. We conclude that also for anatase, our simple bond counting model explains the observed dichroism in A-B peak region.

Table 2: Alignment of nanoribbon principal axes (X,Y,Z) with TiO_2 crystal axes[(1)]

nanoribbon	X	Y	Z
TiO_2-B	a	b	z
anatase	c	ab	ab

[(1)] "ab" means any direction in the (001) plane and "z" is perpendicular to (001). These relations have been obtained from the NEXAFS analysis alone.

Table 2 summarizes the relations, as obtained from the linear dichroism analysis, between TiO_2 crystal axes and the principal axes of the nanoribbons. The results agree with the TEM diffraction measurements (see Supporting Information). The relative orientation between the TiO_2-B and anatase crystal axes has been studied previously at the phase boundary in nanoparticles with TEM[25–27] and theoretical simulations.[27] It was found that the **b**-axes of the two crystal are parallel while the TiO_2-B **a**-axis is aligned with the anatase **c**-axis[26] or vice-versa.[25] These orientational relations are consistent with our assignments in Table 2, when taking account of the tetragonal symmetry in anatase.

Conclusions

In summary, we have studied the electronic structure changes of TiO_2 nanoribbons across the phase transition from TiO_2-B to anatase through polarization dependent NEXAFS and DFT calculations. The O K-edge spectra of individual nanoribbons show strong X-ray linear dichroism which reflects the anisotropic electronic structure around the O sites. We have devised a simple bond counting model which explains the main dichroic effect semi-quantitatively. Further, the orientation of the crystal axes in individual nanoparticles has been found from the analysis of the dichroic spectra alone, and the assignments agree with our electron diffraction data and the literature. This result is particularly promising for soft matter and functionalized nanoparticles where transmission electron microscopy cannot be applied because of radiation damage.

Supporting Information

Details of sample preparation and results of structural characterization, including powder X-ray diffraction patterns, transmission electron microscopy images and diffraction patterns and transmission X-ray microscopy images.

Acknowledgement

We thank the Helmholtz-Zentrum Berlin for the allocation of synchrotron radiation beamtime. The work was partially supported by European Community's Seventh Framework Programme (FP7/2007-2013) under grant agreement n.°312284 (CALIPSO), Programme NanoCF (No. PIRSES-GA-2013-612577) and COST Action EUspec, MP1306, as well as JSPS KAKENHI Grant Number 16K05393. We acknowledge funding by the Belgian Fund for Scientific Research (FRS-FNRS) under the CDR contract FITTED and by the Slovenian Research Agency research program P1-0125. C. B. is a Research Associate at FRS-FNRS.

References

(1) Kasuga, T.; Hiramatsu, M.; Hoson, A.; Sekino, T.; Niihara, K. Formation of Titanium Oxide Nanotube. *Langmuir* **1998**, *14*, 3160-3163.

(2) Armstrong, A. R.; Armstrong, G.; Canales, J.; Bruce, P. G. TiO_2-B Nanowires. *Angew. Chemie Int. Ed* **2004**, *43*, 2286-2288.

(3) Umek, P.; Korošec Cerc, R.; Jančar, B.; Dominko, R.; Arčon, D. The Influence of the Reaction Temperature on the Morphology of Sodium Titanate 1D Nanostructures and Their Thermal Stability. *J. Nanosci. Nanotechnol.* **2007**, *7*, 3502-3508.

(4) Wang, X.; Li, Z.; Shi, J.; Yu, Y. One-Dimensional Titanium Dioxide Nanomaterials: Nanowires, Nanorods, and Nanobelts. *Chem. Rev.* **2014**, *114*, 9346-9384

(5) Morgan, B.J.; Madden, P. A. Lithium Intercalation into TiO_2(B): A Comparison of LDA, GGA and GGA+U Density Functional Calculations. *Phys. Rev. B* **2012**, *86*, 035147.

(6) Ben Yahia, M.; Lemoigno, F.; Beuvier, T.; Filhol, J.-S.; Richard-Plouet, M.; Brohan, L.; Doublet, M.-L. Updated References for the Structural, Electronic, and Vibrational Properties of TiO_2(B) Bulk Using First-Principles Density Functional Theory Calculations. *J. Chem. Phys.* **2009**, *130*, 204501.

(7) Dylla, A. G.; Henkelman, G.; Stevenson, K. J. Lithium Insertion in Nanostructured TiO_2(B) Architectures. *Acc. Chem. Res.* **2013**, *46*, 1104-1112.

(8) Jokisaari, J. R,; Bayer, D.; Zhang, K.; Xie, L.; Nie, Y.; Schlom, G,; Kioupakis, E.; Graham, G. W.; Pan, X. Polarization-Dependent Raman Spectroscopy of Epitaxial TiO_2(B) Thin Films. *Chem. Mater.* **2015**, *27*, 7896-7902.

(9) Felten, A.; Gillon, X.; Gulas, M.; Pireaux, J.-J.; Ke, X.; Van Tendeloo, G.; Bittencourt, C.; Najafi, E.; Hitchcock, A. P. Measuring Point Defect Density in Individual Carbon Nanotubes Using Polarization-Dependent X-ray Microscopy. *ACS Nano* **2010**, *4*, 4431-4436.

(10) Guttmann, P.; Bittencourt, C.; Rehbein, S.; Umek, P.; Ke, X.; Van Tendeloo, G.; Ewels, C. P.; Schneider, G., Nanoscale Spectroscopy with Polarized X-rays by NEXAFS-TXM. *Nature Photonics* **2012**, *6*, 25-29.

(11) Bavykin, D. V.; Friedrich, J. M.; Walsh, F. C. Protonated Titanates and TiO_2 Nanostructured Materials: Synthesis, Properties, and Applications. *Adv. Mater* **2006**, *18*, 2807-2824.

(12) Kiatkittipong, K.; Scott, J.; Amal, R. Hydrothermally Synthesized Titanate Nanostructures: Impact of Heat Treatment on Particle Characteristics and Photocatalytic Properties *ACS Appl. Mater. Interfaces* **2011**, *3*, 3988-3996.

(13) Rutar, M.; Rozman, N.; Pregelj, M.; Bittencourt, C.; Korošec Cerc, R.; Škapin Sever, A.; Mrzel, A.; Škapin, S. D.; Umek, P. Transformation of Hydrogen Titanate Nanoribbons to TiO_2 Nanoribbons and the Influence of the Transformation Strategies on the Photocatalytic Performance. *Beilstein J. Nanotechnol.* **2015**, *6*, 831-844.

(14) Kresse, G.; Furthmüller, J. Efficient Iterative Schemes for Ab Initio Total-Energy Calculations Using a Plane-Wave Basis Set. *Phys. Rev. B* **1996**, *54*, 11169-11186.

(15) Qi, D. C.; A.R. Barman, A. R.; Debbichi, L.; Dhar, S.; Santoso, I.; Asmara, T. C.; Omer, H.; Yang, K.; Krüger, P.; Wee, A. T. S. *et al.* Cationic Vacancies and Anomalous Spectral-Weight Transfer in $Ti_{1-x}Ta_xO_2$ Thin Films Studied Via Polarization-Dependent Near-Edge X-Ray Absorption Fine Structure Spectroscopy. *Phys. Rev. B* **2013**, *87*, 245201.

(16) Bittencourt, C.; Krüger, P.; Lagos, M. J.; Ke, X.; Van Tendeloo, G.; Ewels, C.; Umek P.; P. Guttmann, P. Towards Atomic Resolution in Sodium Titanate Nanotubes Using Near-Edge X-Ray-Absorption Fine-Structure Spectromicroscopy Combined with Multichannel Multiple-Scattering Calculations, *Beilstein J. Nanotechnol.* **2012**, *3*, 789-797.

(17) Zhu, X.; Hitchcock, A.; Bittencourt, C.; Umek, P.; Krüger, P. Individual Titanate Nanoribbons Studied by 3D-resolved Polarization Dependent X-ray Absorption Spectra Measured with Scanning Transmission X-ray Microscopy, *J. Phys. Chem. C* **2015**, *119*, 24192-24200.

(18) Wu, Z. Y.; Ouvrard, G.; Gressier, P.; Natoli, C. R. Ti and O K Edges for Titanium Oxides by Multiple Scattering Calculations: Comparison to XAS and EELS Spectra. *Phys. Rev. B* **1997**, *55*, 10382-10391.

(19) Humar, M.; Arčon, D.; Umek, P.; Škarabot, M.; Muševič, I.; Bregar, G. Mechanical Properties of Titania-Derived Nanoribbons. *Nanotechnology* **2006**, *17*, 3869-3872.

(20) Umek, P.; Bittencourt, C.; Guttmann, P.; Gloter, A.; Škapin, S. D.; Arčon, D. Mn^{2+} Substitutional Doping of TiO_2 nanoribbon: a Three-Step Approach. *J. Phys. Chem C* **2014**, *118*, 21250-21257.

(21) Santar, B.; Giri, P. K.; Dhara, S.; Imakita, K.; Fujii, M. Oxygen Vacancy-Mediated Enhanced Ferromagnetism in Undoped and Fe-Doped TiO_2 Nanoribbons. *J. Phys. D: Appl. Phys.* **2014**, *47*, 235304.

(22) Biener, J; Bäumer, M.; Wang, J.; Madix, R. J. Electronic Structure and Growth of Vanadium on TiO_2(110). *Surf Sci.* **2000**, *450*, 12-26.

(23) Krüger, P. Multichannel Multiple Scattering Calculation of L2,3-edge Spectra of TiO_2 and $SrTiO_3$: Importance of Multiplet Coupling and Band Structure, *Phys. Rev. B* **2010**, *81*, 125121.

(24) de Groot, F. M. F.; Faber, J.; Michiels, J. J. M.; Czyzyk, M. T. ; Abbate, M.; Fuggle, J. C. Oxygen 1s X-Ray Absorption of Tetravalent Titanium Oxides: A Comparison with Single-Particle Calculations. *Phys. Rev. B* **1993**, *48*, 2074-2080.

(25) Yang, D. J.; Liu, H. W.; Zheng, Z. F.; Yuan, Y.; Zhao, J. C.; Waclawik, E. R.; Ke, X. B.; Zhu, H. Y. An Efficient Photocatalyst Structure: TiO2(B) Nanofibers with a Shell of Anatase Nanocrystals. *J. Am. Chem. Soc.* **2009**, *131*, 17885-17893.

(26) Zhou, W.; Gai, L.; Hu, P.; Cui, J.; Liu, X.; Wang, D.; Li, G.; Jiang, H.; Liu, D.; Liu H.; Wang J. Phase Transformation of TiO_2 nanobelts and TiO_2(B)/anatase Interface Heterostructure Nanobelts with Enhanced Photocatalytic Activity. *CrystEngComm* **2011**, *13*, 6643-6649.

(27) Zhu, S.-C,; Xie, S.-H.; Liu Z.-P. Design and Observation of Biphase TiO_2 Crystal with Perfect Junction. *J. Phys. Chem. Lett.* **2014**, *5*, 31623168.

TOC graphic